24th COBEM - 2017

24th ABCM International Congress of Mechanical Engineering
December 3-8, 2017, Curitiba, PR, Brazil

COBEM-2017-1079
EXPERIMENTAL VALIDATION OF AN AMR MODEL FOR MAGNETIC FIELD - FLUID FLOW SYNCHRONIZATION ANALYSIS

Alan Tihiro Dias Nakashima
alan.nakashima@polo.ufsc.br
Sergio Luiz Dutra
sergio.dutra@polo.ufsc.br
Paulo Vinicius Trevizoli
paulot@uvic.ca

Institute for Integrated Energy Systems, Department of Mechanical Engineering, University of Victoria, Victoria, B.C., Canada

Jader Riso Barbosa Jr
jrb@polo.ufsc.br

Polo - Research Laboratories for Emerging Technologies in Cooling and Thermophysics, Department of Mechanical Engineering, Federal University of Santa Catarina, Florianópolis, SC, 88040-900, Brazil

Abstract. *Ideally, active magnetic regenerators (AMR) are based on the thermo-magnetic Brayton cycle, in which the adiabatic magnetic field change processes (magnetization and demagnetization) occur at different periods of the isofield/fluid flow processes (hot and cold blows). In real systems, however, the magnetization and demagnetization steps in general occur simultaneously with the cold and hot blows. As a result, the synchronization between the magnetic field change and fluid flow processes play an important role in the AMR performance, and research is still needed to a better understand of such synchronization. This way, the objective of the present paper is to experimentally validate results of thermal performance of an AMR mathematical model subjected to different fluid flow waveforms and a fixed magnetic field variation. The experimental apparatus consists of a nested Halbach cylinder inside of which the regenerative matrix is assembled. The fluid flow system is composed by a gear pump and a set of rotary valves designed to perform nearly trapezoidal waveforms with different flow periods. The mathematical model of the governing equations for porous media was implemented using the Finite Volume Method. Experimental data for four different flow profiles are used to validate the simulation results.*

Keywords: *magnetic refrigeration, active magnetic regenerator, magnetic field - fluid flow synchronization*

1. INTRODUCTION

An active magnetic regenerator (AMR) based on the thermo-magnetic Brayton cycle performs four steps (Rowe *et al.*, 2005): (i) adiabatic magnetization: by adiabatically changing the magnetic field applied on the regenerator, the temperature of the magnetocaloric material (MCM) increases due to the magnetocaloric effect (MCE); (ii) cold blow: fluid from the cold reservoir flows through the porous matrix composed of MCM, removing heat to be rejected at a hot reservoir; (iii) adiabatic demagnetization: removal of the field reduces the temperature of the MCM (reversible MCE); (iv) hot blow: fluid from the hot reservoir flows through the matrix, where it is cooled down to absorb heat from a cold reservoir. Fig. 1 presents a schematic diagram of the cycle and the main components of a AMR system.

AMR prototypes usually perform steps (i) and (ii), as well steps (iii) and (iv), simultaneously. Previous works have numerically (Bjørk and Engelbrecht, 2011; Trevizoli *et al.*, 2014a; Plaznik *et al.*, 2013), and experimentally (Plaznik *et al.*, 2013; Teyber *et al.*, 2016) demonstrated that it is possible to increase the performance of an AMR by changing the fluid flow waveform synchronization with respect to the magnetic field waveform. None of those works, however, performed an experimental assessment with validation of a numerical model aiming at finding optimum synchronization parameters.

This way, the present work advances on the experimental evaluation of the magnetic field and flow waveforms synchronization, which was carried out in the AMR test apparatus developed by Trevizoli *et al.* (2016b) and adapted by Nakashima (2017). The experimental characterization is performed based on data for cooling capacity, temperature spans and pressure drop, which were used to validate the 1D and transient mathematical model of an AMR proposed by Trevizoli *et al.* (2016a). The model is composed by the momentum equation for porous media, and the solid and fluid energy

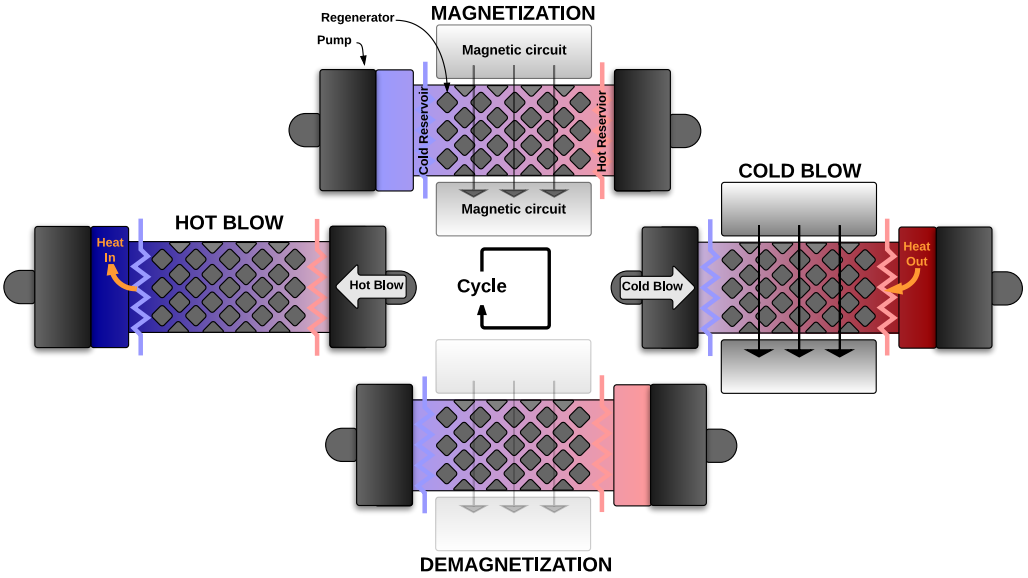

Figure 1. Schematic diagram of the Brayton thermo-magnetic cycle (Trevizoli, 2015).

equations which are solved couple. The finite volume method with a fully implicit scheme is used. The magnetocaloric effect is directly included in the solid energy equation as a finite adiabatic temperature change (Nielsen *et al.*, 2011). The results showed reasonable agreement between the numerical and experimental average cooling capacities, as the numerical data were within +/- 20% range for different blow time fractions,F_{B}, which is defined as the ratio of blow and the total cycle periods. Transient temperature and pressure drop results were also successfully reproduced by the numerical model.

2. EXPERIMENTAL METHOD

The experimental apparatus for AMR evaluation (Fig. 2) was developed by Trevizoli *et al.* (2016b) and adapted by Nakashima (2017) in order to enable F_{B} variation, and its schematic diagram is presented in Fig. 3(a). A new pumping system composed by a gearpump and a set of two rotary valves were installed to replace the previous piston-based pumping system. The high pressure valve (HPV) is responsible for delivering fluid from the gearpump to the AMR main lines (cold and hot lines) during blow periods, as well diverting the working fluid when no-flow periods are required. Adjustment of the no-flow duration allows the assessment of four different flow waveforms or F_{B}: 50%, 45%, 40% and 32.5%. The low pressure valve (LPV) returns fluid form the main lines to the reservoir. The cold line also includes a balancing valve before the regenerator entrance, whose function is to control the total mass delivered during the cold blow and, thus, correct any mass imbalance between cold and hot blows, which results in performance loss if not minimized (Eriksen *et al.*, 2016; Teyber *et al.*, 2016; Nakashima *et al.*, 2017).

The magnetic circuit is composed of nested Halbach Cylinders (HCC), whose counter-rotation enables magnetic flux density (in this work called magnetic field, B) variation in its bore following a rectified sinusoidal waveform. Fig. 4 presents the transient mass flow rate and B waveforms evaluated in this work. The regenerator bed is composed by a packed bed matrix with 0.55 mm commercial grade gadolinium (Gd) spheres, in a total of 194.77 g and porosity of 0.364. The bed is placed in the bore of the magnetic circuit. Thermal baths are used to control the AMR entrance temperatures, T_{C} and T_{H}, and thus, the temperature span is $\Delta T_{\mathrm{span}} = T_{\mathrm{H}} - T_{\mathrm{C}}$. Thermal contact between fluid from the bath and the working fluid of the apparatus is enabled by two brazed plate heat exchangers.

Calibrated thermocouples (Omega TMQSS-020G, uncertainty of 0.15 K) were placed at several positions (as shown in Fig. 2) and the main ones located at the regenerator ends (cold and hot ends) were used to evaluate the cooling capacity, $\dot{Q}_{\mathrm{c}}$, as follows:

$$\dot{Q}_{\mathrm{C}} = \frac{1}{\tau}\int_{\tau_{HB}} \overline{\dot{m}}_{HB}(t) c_{\mathrm{p,f}} (T_{\mathrm{C}}(t) - T_{\mathrm{CHEX}}) dt \simeq \frac{\tau_{\mathrm{HB}} \overline{\dot{m}}_{\mathrm{HB}} c_{\mathrm{p,f}}}{\tau} \overline{\Delta T}_{\mathrm{C}} \tag{1}$$

where τ and τ_{HB} are the cycle and hot blow periods, $\overline{\dot{m}}_{HB}$ is the average mass flow rate during the hot blow, $c_{\mathrm{p,f}}$ is the fluid specific heat, $T_{\mathrm{C}}(t)$ and T_{CHEX} are the cold thermal reservoir and AMR exit temperatures during the hot blow, respectively. $\overline{\Delta T}_{\mathrm{C}}$ is the average difference between $T_{\mathrm{C}}(t)$ and T_{CHEX} during hot blow.

Coriolis flow transducers (Krone Optimass 3300C, uncertainty of 1%) were used to measure mass flow rate during each blow and pressure transducers (Omega PX613, uncertainty of 0.5 kPa) enabled the calculation of the pressure drop along the regenerative bed. A linear potentiometer actuated by the stepper motor is used to calculate cycle frequency and

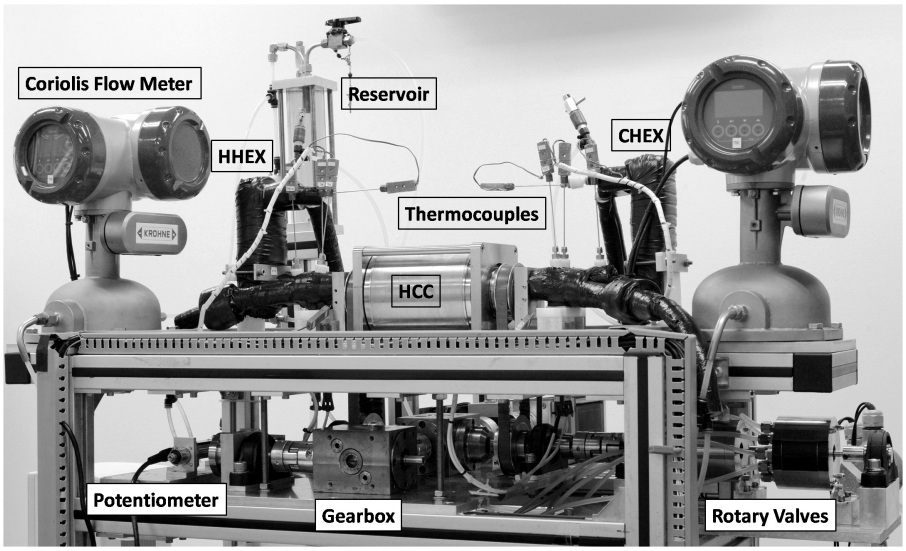

Figure 2. Main components of the experimental apparatus (Nakashima *et al.*, 2017).

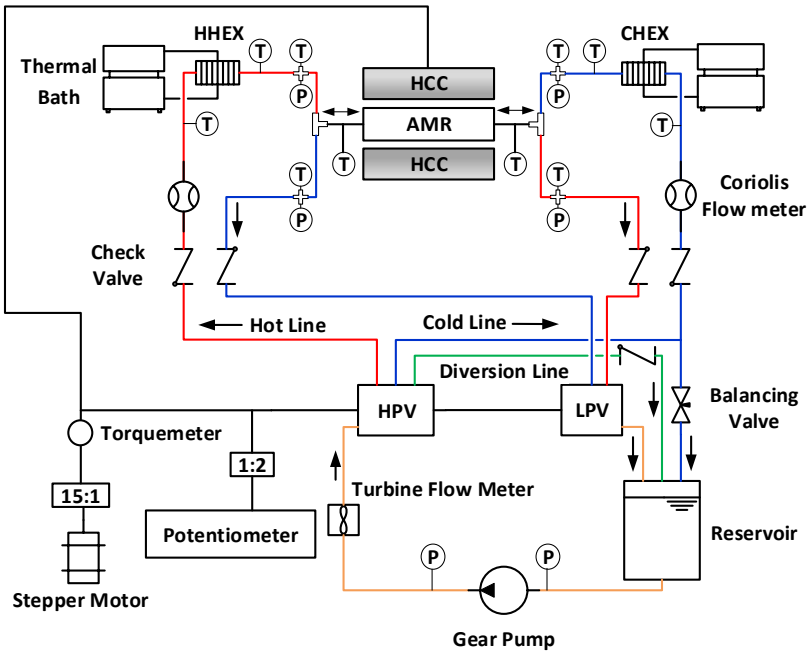

Figure 3. Schematic diagram of the experimental apparatus (arrows indicate the flow direction) (Nakashima *et al.*, 2017).

a torque meter (HBM T22/50Nm, uncertainty of 0.5%) measures the total torque input required by the apparatus. The experimental procedure started by setting cycle frequency, blow time fraction, utilization factor, ϕ (defined as the ratio of fluid and solid thermal capacities during the hot blow), and reservoir temperatures. The first point is measured at zero ΔT_{span}, and the subsequent tests conditions are achieved by increasing ΔT_{span} up to 15 K in 5 K steps. Mass imbalance was corrected each step following the criteria established in Nakashima *et al.* (2017). The average expanded uncertainties of the temperature span and utilization factor have been calculated as 0.3 K and 0.01, respectively. Although relative uncertainties of $\dot{Q}_{\text{c}}$ are high (over 20 %), the experimental apparatus and methods described here presented consistent results throughout several previous analysis and investigations (Trevizoli *et al.*, 2014b, 2016b, 2017).

3. MATHEMATICAL MODEL

The governing equations of fluid flow (momentum equation) and heat transfer between the porous matrix and working fluid (solid and fluid energy equations) were solved by a Finite Volume Method transient routine under the following assumptions: incompressible flow, low porosity and body forces absence. The geometric domain of solution is presented

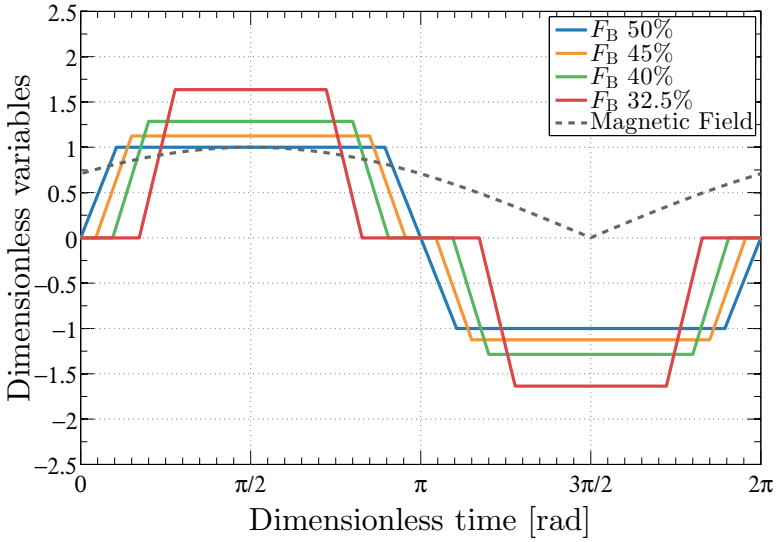

Figure 4. Effects of different F_{B} on the mass flow rate and magnetic field waveforms.

in Fig. 5 includes the regenerator porous matrix as well as regenerator casing and the air gap, whose energy balance equations are solved to simulate heat gain/loss from/to the surroundings (Trevizoli *et al.*, 2016a; Trevizoli and Barbosa Jr., 2017).

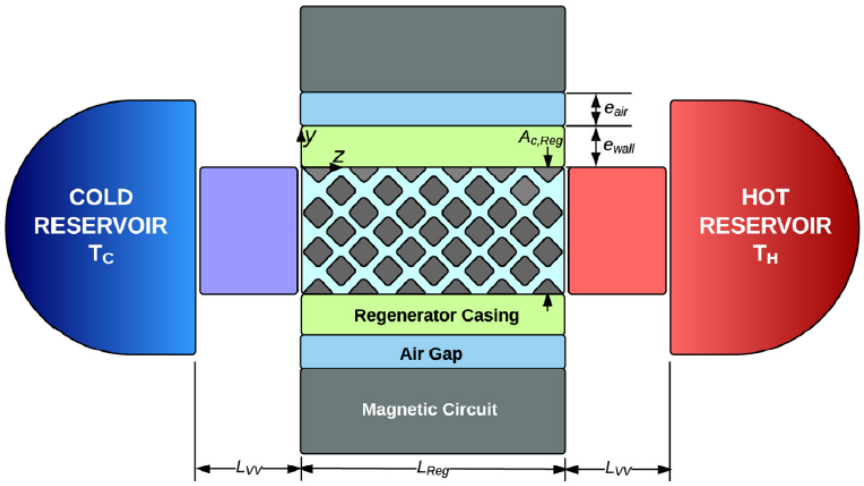

Figure 5. Geometric domain of solution of the AMR model. Adapted from (Trevizoli *et al.*, 2016a).

The simplified momentum equation, also known as Brinkman-Forchheimer equation is (Kaviany, 1995; Nield and Bejan, 2006):

$$\frac{\rho_{\mathrm{f}}}{\varepsilon}\left(\frac{\partial u}{\partial t}\right) = -\frac{\partial P}{\partial z} - \frac{\mu_{\mathrm{f}}}{K}u - \frac{c_{\mathrm{E}}\rho_{\mathrm{f}}}{K^{1/2}}|u|u \tag{2}$$

where ρ_f is the density, u is the z component of the Darcian velocity, P is pressure, μ_{f} the dynamic viscosity. K and c_E are the permeability and Ergun constant found in Ergun (1952). Left hand term accounts for the transient effects, and the right hand terms are the pressure gradient, microscopic viscous tension and microscopic inertia respectively. The pressure gradient is a transient function that imposes the trapezoidal and oscillatory nature of the flow (Zhao and Cheng, 1996; Oliveira *et al.*, 2012; Trevizoli and Barbosa Jr., 2017). As this term is a input of the solution, the momentum equation written as the Eq. 2 returns only one value of u as a possible solution each time step.

The simplied solid energy equation is:

$$\rho_{\mathrm{s}}(T)c_{\mathrm{s}}(T)(1-\varepsilon)\frac{\partial T_{\mathrm{s}}}{\partial t} = h(z)\beta(T_{\mathrm{f}} - T_{\mathrm{s}}) + (1-\varepsilon)k_{\mathrm{s}}^{\mathrm{eff}}\frac{\partial^2 T_{\mathrm{s}}}{\partial z^2} \tag{3}$$

where ρ_{s}, c_{s}, $k_{\mathrm{s}}^{\mathrm{eff}}$ and T_{s} are the density, specific thermal capacity, effective thermal conductivity and temperature of the solid, respectively. T_{f} is the fluid temperature, β is the interstitial heat transfer area and regenerator volume ratio and h is the interstitial heat transfer coefficient. The transient terms are on the left side of the equation, while the interstitial heat transfer and the axial conduction are on the right side. The expression for $k_{\mathrm{s}}^{\mathrm{ef}}$ for a packed bed of spheres can be found in Hadley (1986). The interstitial heat transfer term couples the solid and fluid energy equations, and requires a Nusselt correlation, which the one proposed by Pallares and Grau (2010) presented a very good agreement with heat transfer data for thermal regenerators composed by packed beds as in Trevizoli and Barbosa Jr. (2017).

Eq. 3 does not present a explicit magnetocaloric effect term, as the EMC is included before each time step calculation as finite adiabatic temperature variation ΔT_{ad} (Nielsen *et al.*, 2011). Magnetic and caloric properties of the solid were calculated from magnetization and specific thermal capacity data measured from a sample of the material. Thermal conductivity and density can be found in Petersen *et al.* (2008).

The fluid energy equation is:

$$\rho_{\mathrm{f}}(T)c_{\mathrm{p,f}}(T)\left(\varepsilon\frac{\partial T_{\mathrm{f}}}{\partial t}+u\frac{\partial T_{\mathrm{f}}}{\partial z}\right)=h(z)\beta(T_{\mathrm{s}}-T_{\mathrm{f}})+\left|u\frac{\partial P}{\partial z}\right|+\varepsilon\left[k_{\mathrm{f}}^{\mathrm{ef}}+\rho_{\mathrm{f}}(T)c_{\mathrm{p,f}}(T)D_{||}\right]\frac{\partial^2 T_{\mathrm{f}}}{\partial z^2}+\dot{q}_{\mathrm{ca}} \tag{4}$$

where $c_{\mathrm{p,f}}$ is the fluid specific heat, $k_{\mathrm{f}}^{\mathrm{ef}}$ and $D_{||}$ are the effective conductivity and dispersion coefficient, found in Kaviany (1995) and Koch and Brady (1985). Left hand terms are transient and advection effects, while the right hand terms are the interstitial heat transfer, viscous dissipation, axial heat conduction and thermal dispersion. Physical properties of the working fluid were obtained from the *software* Engineering Equation Solver (EES) properties library (Klein, 2013).

The $\dot{q}_{\mathrm{ca}}$ term in Eq. 4 accounts for the heat loss from the regenerator to the magnetic circuit, which is assumed as a constant temperature medium kept at the ambient temperature of 300 K due to its high thermal mass. $\dot{q}_{\mathrm{ca}}$ is calculated after the solution of the 2D energy equations of the regenerator casing and air gap between the AMR and magnetic circuit. Nusselt correlation for convective heat transfer boundary condition at the porous medium and casing interface can be found in Li and Finlayson (1977). Demagnetization losses which reduces the effective magnetic field applied to the AMR were also included, and further details for the loss implementation and routine solution can be found in Trevizoli *et al.* (2016a). The analyzed parameters are the same as in the experimental procedure. The model was able to calculate the $\dot{Q}_{\mathrm{c}}$ developed by the AMR as well as the transient temperature and pressure drop, which were compared to the experimental results.

4. RESULTS AND DISCUSSION

Fig. 6 shows validation data comparing the experimental and numerical cooling capacities for mass balanced conditions simulated in the model. For both frequencies evaluated, the model over predicted most of the data points because the imbalance criteria established for the experimental tests accepted a certain degree of imbalance in favour of the hot blow fluid mass, which results in lower cooling capacities. The imbalance criteria for the experiments was a hot blow total mass 1% to 3% higher than the cold blow (Nakashima *et al.*, 2017). After the inclusion of the same imbalance criteria on the mathematical model by increasing the hot blow mass flow rate, the overall agreement was improved, as presented in Fig. 7. The validation results for 0.25 Hz (Fig. 7 (a)) showed a more even distribution inside the 20% region, with some points outside.

At 0.5 Hz (Fig. 7 (b)), the data points lied above the centreline of the 20% region even after the inclusion of the mass imbalance, and most of the ΔT_{span} 15 K results were overestimated by more than 20% even with the inclusion of mass imbalance. As explained in Trevizoli *et al.* (2016a), the agreement of model predictions when the cycle frequency rises is expected to decrease, because additional losses are not modelled (e.g heat generated by friction at bearings). Moreover, void volume effects (Trevizoli and Barbosa Jr., 2017) were not included in the present simulations in order to reduce computational resource requirements, however, the impact of such losses is more pronounced exactly at higher values of temperature span (Trevizoli *et al.*, 2016a). Therefore, inclusion of void volume is recommend despite its computational cost. Nevertheless, Fig. 8 presents the AMR characteristic curves associated with two sets of experimental data and the respective model results with and without the inclusion of the mass imbalance (unbalanced and balanced conditions, respectively). It can be seen that, overall, the model is able to predict the experimental trend and also reproduce the effects of mass imbalance. The inclusion of the void volume would improve results for higher ΔT_{span}.

Validity of the model is further confirmed by the transient temperature and pressure drop results. Fig. 9 (a) and (b) shows transient measurements and numerical results of the temperature at the cold regenerator end as a function of the dimensionless time, $t^* = 2\pi f t$. From 0 to π, the temperatures converge to the cold reservoir temperature T_{c} as the system is performing the cold blow. During the hot blow (π to 2π), the exit temperatures are initially lower than T_{c}, but due to limited effectiveness of the matrix and positive magnetic field variation, the temperature rises above T_{c} and the cooling capacity reduces, as it is proportional to $\overline{\Delta T}_{\mathrm{C}}$ (Eq. 1). Moreover, the inclusion of mass imbalance in Fig. 9 (a) improved the numerical predictions, while in Fig. 9 (b) it increased the difference as the balanced simulation were already over predicting the experimental results.

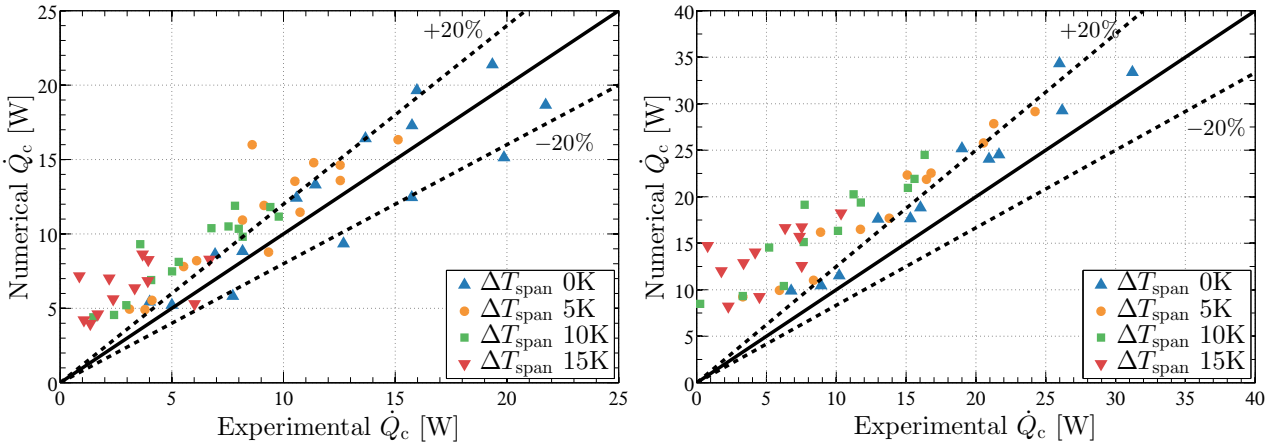

Figure 6. Experimental and numerical cooling capacity comparison for balanced simulated conditions at (a) 0.25 Hz and (b) 0.5 Hz.

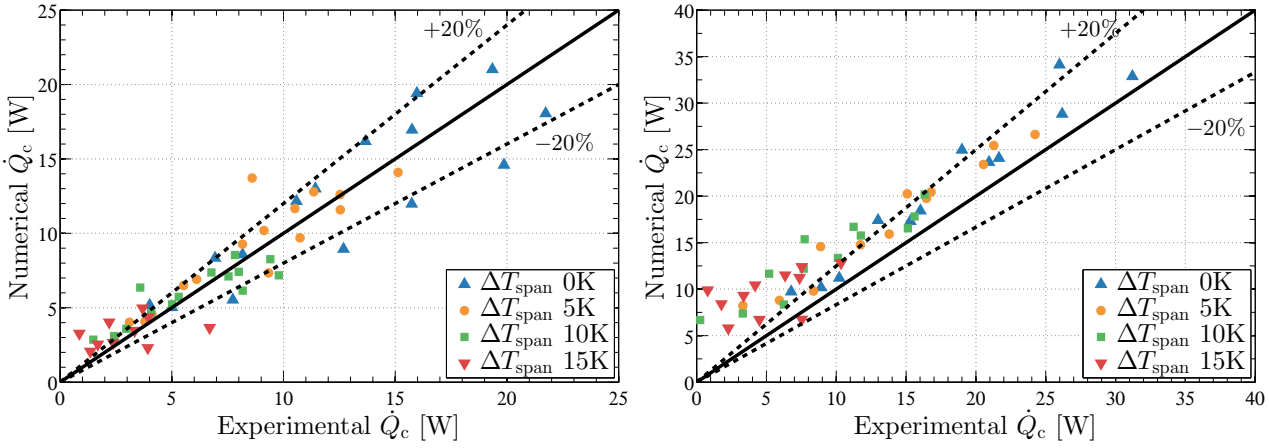

Figure 7. Experimental and numerical cooling capacity comparison after the inclusion of the mass imbalance criteria in the simulated conditions at (a) 0.25 Hz and (b) 0.5 Hz.

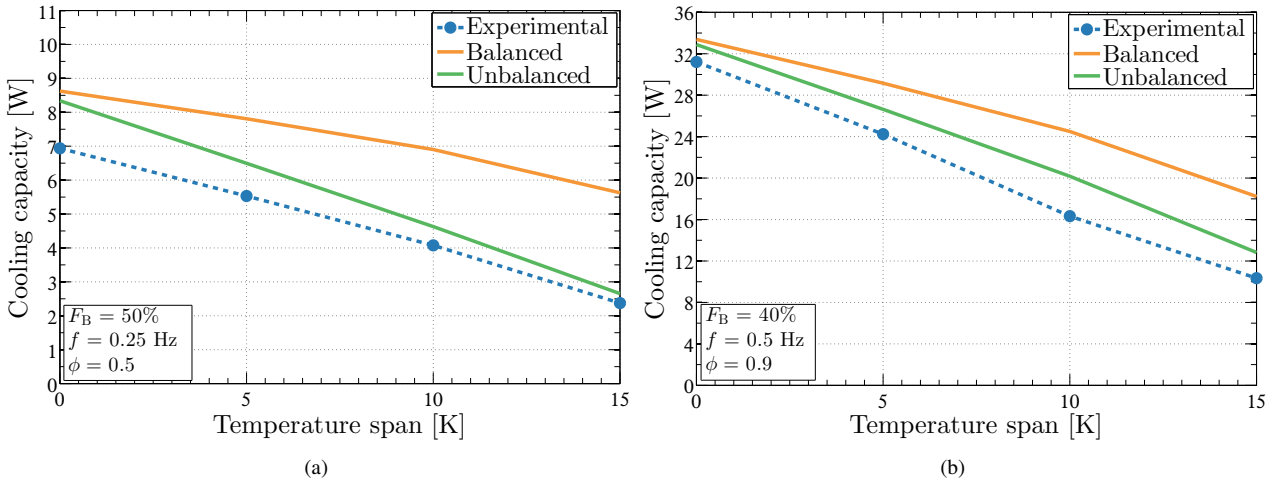

Figure 8. Characteristic AMR curves for two experimental test conditions and the respective numerical balanced and unbalanced results.

In addition, there is a difference between theoretical and real regenerator pressure drop waveforms presented in Fig. 10 for two test conditions. The experimental ΔP is not an ideal trapezoid and the flow direction change is smooth instead of the sharp idealized pressure input of the model. Hot and cold blows periods are not equal as the numerical model

assumes due to the torque oscillations described in section 2. Peak values of pressure drop in the apparatus is also higher because of the auxiliary tubing and hydraulic connections. Nevertheless, the idealization of the fluid flow is a reasonable approximation for AMR numerical evaluation (Trevizoli, 2015) which saves computational cost of the solution.

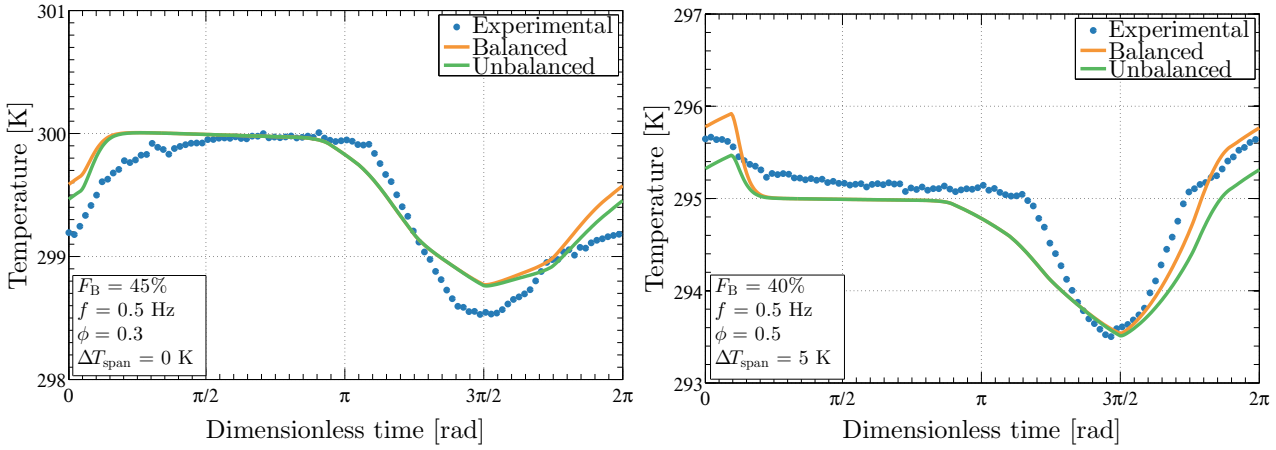

(a) (b)

Figure 9. Regenerator cold end temperature for two experimental test conditions and the respective numerical balanced and unbalanced results.

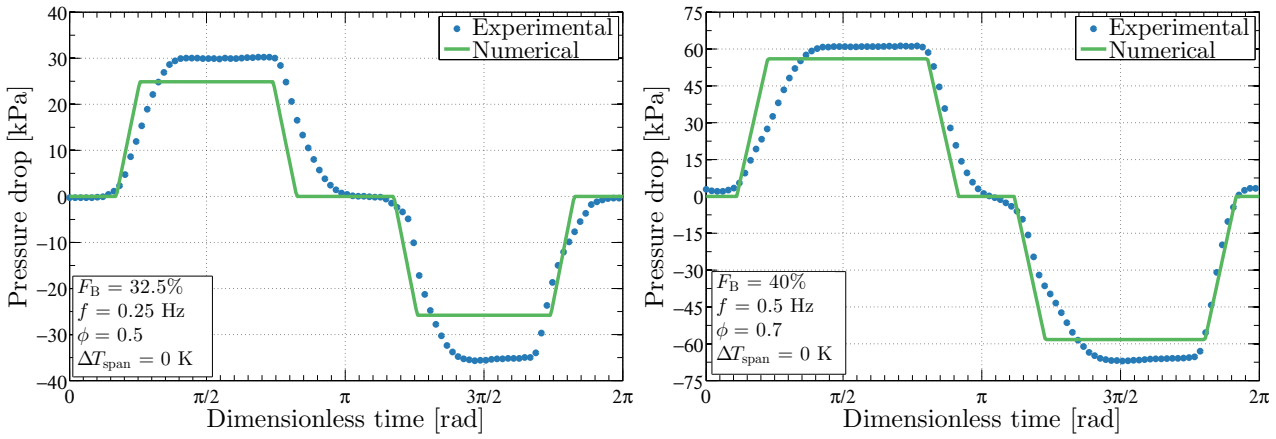

(a) (b)

Figure 10. Regenerator pressure drop for two experimental test conditions and the respective numerical balanced and unbalanced results.

5. CONCLUSIONS

A 1D AMR numerical model was validated with respect to the inclusion of different flow waveforms and synchronization between fluid flow and magnetic field variation. Numerical cooling capacity and transient profiles were compared to experimental data and both showed good agreement. The average cooling capacity comparison revealed the necessity of void volume losses inclusion in order to improve numerical results for higher temperature spans. It is not clear why the model performance is reduced for higher frequencies, and future investigations should focus on the inclusion of other losses mechanisms as heat leaks if more accurate results are required. Another solution is the modelling of the main hydraulic components of the apparatus and in order to input more accurate pressure drop waveforms in the numerical AMR routine. Nevertheless, despite quantitative differences regarding the experimental results, which were anticipated due to the apparatus complexity, the model developed by Trevizoli *et al.* (2016b) is suitable for future optimization analysis concerning fluid flow and magnetic field waveforms synchronization.

6. ACKNOWLEDGMENTS

Financial support from CNPq, CAPES, Embraco and the EMBRAPII Unit Polo/UFSC is duly acknowledged.

7. REFERENCES

Bjørk, R. and Engelbrecht, K., 2011. "The influence of the magnetic field on the performance of an active magnetic regenerator (AMR)". *International Journal of Refrigeration*, Vol. 34, pp. 192–203.

Ergun, S., 1952. "Fluid flow through packed columns". *Chem. Process Eng. London*, Vol. 48, pp. 89–94.

Eriksen, D., Engelbrecht, K., Bahl, C.R.H., Bjørk, R. and Nielsen, K.K., 2016. "Effects of flow balancing on active magnetic regenerator performance". *Applied Thermal Engineering*, Vol. 103, pp. 1–8.

Hadley, G.R., 1986. "Thermal conductivity of packed metal powder". *International Journal of Heat and Mass Transfer*, Vol. 29, pp. 909–920.

Kaviany, M., 1995. *Principles of Heat Transfer in Porous Media*. Springer, 2nd edition.

Klein, S.A., 2013. "Engineering Equation Solver (EES) Professional Version". V9.339, F-Chart Software, Madison, WI.

Koch, D.L. and Brady, J.F., 1985. "Dispersion in fixed beds". *Journal of Fluid Mechanics*, Vol. 154, pp. 399–427.

Li, C.H. and Finlayson, B.A., 1977. "Heat transfer in packed beds - a reevaluation". *Chemical Engineering Science*, Vol. 32, pp. 1055–1066.

Nakashima, A.T.D., 2017. *Avaliação Teórica e Experimental da Influência do Perfil Temporal do Escoamento sobre a Performance de um Regenrador Magnético-Ativo*. Master's thesis, Universidade Federal de Santa Catarina.

Nakashima, A.T.D., Dutra, S.L., Trevizoli, P.V. and Barbosa Jr., J.R., 2017. "Experimental evaluation of the flow imbalance in an active magnetic regenerator".

Nield, D.A. and Bejan, A., 2006. *Convection in Porous Media*. 3rd edition.

Nielsen, K.K., Tusek, J., Engelbrecht, K., Schopfer, S., Kitanovski, A., Bahl, C.R.H., Smith, A., Pryds, N. and Poredos, A., 2011. "Review on numerical modeling of active magnetic regenerators for room temperature applications". *International Journal of Refrigeration*, Vol. 34, pp. 603–616.

Oliveira, P.A., Trevizoli, P.V., Barbosa Jr., J.R. and Prata, A.T., 2012. "A 2D hybrid model of the fluid flow and heat transfer in a reciprocating active magnetic regenerator". *International Journal of Refrigeration*, Vol. 35, pp. 98–114.

Pallares, J. and Grau, F.X., 2010. "A modification of a nusselt number correlation for forced convection in porous media". *International Communications in Heat and Mass Transfer*, Vol. 37, pp. 1187–1190.

Petersen, T.F., Engelbrecht, K., Bahl, C.R.H., Elmegaard, B., Pryds, N. and Smith, A., 2008. "Comparison between a 1D and a 2D numerical model of an active magnetic regenerative refrigerator". *Journal of Physics D: Applied Physics*, Vol. 41, pp. 105002(1–8).

Plaznik, U., Tušek, J., Kitanovski, A. and Poredoš, A., 2013. "Numerical and experimental analyses of different magnetic thermodynamic cycles with an active magnetic regenerator". *Applied Thermal Engineering*, Vol. 59, pp. 52–59.

Rowe, A., Tura, A., Dikeos, J. and Chahine, R., 2005. "Near room temperature magnetic refrgeration". In *Proceedings of the International Green Energy Conference*.

Teyber, R., Trevizoli, P., Niknia, I., Christiaanse, T., Govindappa, P. and Rowe, A., 2016. "Experimental performance investigation of an active magnetic regenerator subject to different fluid flow waveforms". *International Journal of Refrigeration*, Vol. 74, pp. 38 – 46.

Trevizoli, P.V., 2015. *Development of Thermal Regenerators for Magnetic Cooling Application*. Ph.D. thesis, Universidade Federal de Santa Catarina.

Trevizoli, P.V. and Barbosa Jr., J.R., 2017. "Thermal-hydraulic behavior and influence of carryover losses in oscillating-flow regenerators". Vol. 113, pp. 89–99.

Trevizoli, P.V., Barbosa Jr., J.R., Tura, A., Arnold, D. and Rowe, A., 2014a. "Modeling of thermo-magnetic phenomena in active magnetocaloric regenerators". *Journal of Thermal Science and Engineering Applications*, Vol. 6, pp. 031016 (1–10).

Trevizoli, P.V., Liu, Y., Tura, A., Rowe, A. and Barbosa Jr., J.R., 2014b. "Experimental assessment of the thermal-hydraulic performance of packed-sphere oscillating-flow regenerators using water". *Experimental Thermal and Fluid Science*, Vol. 57, pp. 324–334.

Trevizoli, P.V., Nakashima, A.T. and Barbosa Jr., J.R., 2016a. "Performance evaluation of an active magnetic regenerator for cooling applications - part ii: mathematical modeling and thermal losses". *International Journal of Refrigeration*, Vol. 72, pp. 206 – 217.

Trevizoli, P.V., Nakashima, A.T., Peixer, G.F. and Barbosa Jr., J.R., 2016b. "Performance evaluation of an active magnetic regenerator for cooling applications - part i: Experimental analysis and thermodynamic performance". *International Journal of Refrigeration*, Vol. 72, pp. 192 – 205.

Trevizoli, P.V., Nakashima, A.T., Peixer, G.F. and Barbosa Jr., J.R., 2017. "Performance assessment of different porous matrix geometries for active magnetic regenerators". *Applied Energy*, Vol. 187, pp. 847 – 861.

Zhao, T. and Cheng, P., 1996. "Oscillatory heat transfer in a pipe subjected to a laminar reciprocating flow". *ASME Journal of Heat Transfer*, Vol. 118, pp. 592–598.

8. RESPONSIBILITY NOTICE

The authors are the only responsible for the printed material included in this paper.